Continuous imaging of amino-acid translocation in intact mycelia of *Phanerochaete velutina* reveals rapid, pulsatile fluxes

M. Tlalka, S. C. Watkinson, P. R. Darrah and M. D. Fricker

Department of Plant Sciences, University of Oxford, South Parks Road, Oxford OX1 3RB, UK

Author for correspondence:
S. C. Watkinson
Tel: +44 (0) 1865 275 119
Fax: +44 (0) 1865 275 074
Email: sarah.watkinson@plants.ox.ac.uk

Received: *27 June 2001*
Accepted: *17 September 2001*

Summary

• Nitrogen translocation by woodland fungi is ecologically important, however, techniques to study long-distance amino-acid transport in mycelia currently have limited spatial and temporal resolution. We report a new continuous, noninvasive imaging technique for β-emitters that operates with submillimetre spatial resolution and a practical sampling interval of 10–60 min.

• Transport of the nonmetabolized, ^{14}C-labelled amino-acid analogue, α-aminoisobutyric acid (AIB) was imaged using a photon-counting camera as it was transported in foraging mycelium of the cord-forming woodland fungus, *Phanerochaete velutina*, grown over an intensifying screen in microcosms.

• The maximum acropetal transport velocity of ^{14}C-AIB to the colony margin was 50 mm h^{-1} (average 23 mm h^{-1}), with a mass transfer of 4.6–51.5 pmol ^{14}C-AIB h^{-1} per cord. Transport in cords had a pulsatile component with a period of 11–12 h.

• Transport was significantly faster than diffusion, consistent with rapid cycling of nutrients throughout the mycelium between loading and sink regions. The increased spatial and temporal resolution of this method also revealed the rhythmic nature of transport in this fungus for the first time.

Key words: *Phanerochaete velutina*, amino-acid transport, scintillation imaging.

Introduction

The mechanism(s) by which fungal mycelia accumulate and translocate nitrogen, and the signalling systems that operate to re-deploy resources where required (Boddy, 1993, 1999; Watkinson, 1999) are not fully understood. Transport of nitrogen compounds in fungal mycelium associated with plant roots (Perez-Moreno & Read, 2000) and litter (Watkinson *et al.*, 1981; Cromack & Caldwell, 1992; Boddy & Watkinson, 1995; Miller & Lodge, 1997) is important in soil nitrogen cycling. Foraging mycelia of many fungi differentiate nutrient-transporting cords, strands or rhizomorphs (Jennings & Watkinson, 1982; Cairney *et al.*, 1989) as the colony advances with characteristic fractal dimensions dependent on species and environment (Boddy *et al.*, 1999).

Rates of nutrient movement through cords are too fast to be accounted for by diffusion alone (Jennings, 1987, 1994; Wells & Boddy, 1990; Olsson & Gray, 1998) and there is evidence for both pressure-driven mass flow (Amir *et al.*, 1995; Brownlee & Jennings, 1982; Cairney, 1992), and cytoplasmic streaming (Harley & Smith, 1983; Cairney, 1992) possibly involving peristalsis through dynamic tubular vacuolar systems (Shepherd *et al.*, 1993; Cole *et al.*, 1998) or vesicle translocation on cytoskeletal elements (Steinberg, 1998; Seiler *et al.*, 1999). Fungi are known to accumulate arginine and ornithine in vacuoles (Weiss, 1973; Ohsumi & Anraku, 1981; Kitamoto *et al.*, 1988), and dynamic rearrangements of the vacuolar membrane have been shown to be involved in the environmentally controlled balance between protein synthesis and degradation in fungal cells (Klionsky & Ohsumi, 1999), suggesting that the vacuolar system is a candidate for the nitrogen transporting compartment within hyphae.

These different transport systems may act in combination as nutrient translocation may involve both cytoplasmic and apoplastic compartments at different stages in the loading, transport and unloading pathway (Cairney, 1992). Multiple

parallel or circulating pathways may be required to accommodate the observed simultaneous acropetal and basipetal nutrient movement in the same rhizomorph or mycelial cord (Granlund *et al.*, 1985; Wells *et al.*, 1998b; Olsson, 1999; Lindahl *et al.*, 2001).

One problem that has hampered direct investigation of nitrogen transport, in comparison with other nutrients such as phosphorus and carbon, is the absence of a convenient radioisotope. Most studies have used ^{15}N and measured transport velocities or fluxes by mass spectrometry (Arnebrandt *et al.*, 1993; Ek *et al.*, 1996). An alternative possibility is to use ^{3}H or ^{14}C-labelled N-compounds. This approach only provides unequivocal evidence for N-translocation if the compound selected reliably follows the normal pathway for natural N-compounds and is not metabolized by the fungus. One such compound is 2-amino[1–^{14}C]isobutyric acid (AIB), a methylated analogue of alanine, which is actively transported into the cell by amino-acid transport proteins (Ogilvie-Villa *et al.*, 1981) and accumulated without being metabolized or incorporated into protein (Kim & Roon, 1982). It is translocated by many fungal species without being metabolized (Watkinson, 1984a; Lilly *et al.*, 1990; Olsson & Gray, 1998). As AIB is not metabolized, the labelled carbon atom is neither lost as carbon dioxide, nor incorporated into protein or cell wall material. Instead it accumulates in the expandable free amino acid pool that is a characteristic feature of fungi (Venables & Watkinson, 1989; Griffin, 1994), and can be translocated through mycelium in this form (Watkinson, 1984b).

A second problem in analysing the dynamics of N-translocation in mycelium has been the difficulty of tracking the transported substance with sufficient time and spatial resolution to define the pathways and mechanisms underlying movement and to follow the dynamic changes that occur as the colony adjusts to changing source-sink patterns. Movement of ^{14}C-AIB has previously been analysed by both destructive sampling techniques (Watkinson, 1984a; Lilly *et al.*, 1990) and imaging using a β-scanner (Olsson & Gray, 1998).

In this paper we describe a new, continuous method for mapping β-emissions from ^{14}C that takes advantage of the ability of foraging fungi to grow over inert surfaces, in this case a scintillation screen. For this work we used the fungus *Phanerochaete velutina*, because it has a pattern of extensive and responsive mycelial growth typical of a woodland cord forming fungus and the ecology of its foraging behaviour and nutrient translocation, particularly of phosphate, has been intensively investigated (Wells *et al.*, 1990; Wells *et al.*, 1995; Wells *et al.*, 1998b; Wells *et al.*, 1998b; Wells *et al.*, 1999). In this report, the new imaging technique was used to determine the speed at which ^{14}C-AIB was translocated through developing cords. These measurements are a prerequisite to define the mechanism(s) and cellular transport routes that might be capable of sustaining N-fluxes *in vivo*.

Materials and Methods

Organism

Cultures of *Phanerochaete velutina*, originally isolated from the field, were kindly provided by Prof. L. Boddy, University of Cardiff, UK. Cultures were maintained on 2% malt agar (2% Oxoid malt extract, 2% Oxoid No. 3 agar) at 22 ± 1°C in the dark in a temperature-controlled incubator (Gallenkamp, England).

Experimental microcosms

For each experiment, an inoculum disc (18 mm diameter) of *P. velutina* cut submarginally from a growing colony on 2% malt agar was placed in the middle of an intensifying screen (Lite Plus, Sigma, Poole, UK) that had been cut to fit a square (120 mm × 120 mm) Petri dish. A small (1 mm) predrilled hole was present in the lid of the Petri dish just over the inoculum disc to allow injection of radioactive label and covered with Parafilm (American National Can™, Neenah, NI, USA) to reduce evaporation. In addition, 1–2 small containers containing 500 µl of water each were placed in the corners of the Petri-dish and the whole dish was sealed with Parafilm to maintain a high relative humidity level (Fig. 1a). To follow amino-acid distribution accompanying growth of mycelium, ^{14}C-AIB was added to the inoculum disc as soon as it had been placed in the dish and then the chamber transferred to the imaging enclosure. To study amino-acid translocation in established mycelium, the chamber was maintained in darkness at 22 ± 1°C in the incubator for 14–21 d until the mycelium had grown at least 30 mm in all directions.

Visualization of ^{14}C-AIB transport using photon-counting scintillation imaging

The β-emitting compound 2-amino[1–^{14}C]isobutyric acid (^{14}C-AIB) was used to label the free amino acid pool in mycelium. In each experimental Petri dish, 50 µl (0.0925 MBq) of a 0.9 mM solution of ^{14}C-AIB (Amersham, UK) in distilled water (specific activity 2.11 GBq mmol^{-1}) was applied to the inoculum disc through the hole in the lid, and the hole re-sealed with Parafilm. Labelled cultures were placed in a light-tight imaging enclosure. The temperature in the enclosure was monitored using 'Diligence'™ data loggers (Comark Ltd, Cambridge, UK). Most experiments were conducted at 23 ± 1°C. The temperature varied slightly from experiment to experiment. The minimum was 19°C and the maximum was 26°C.

Light emission from the radiation-sensitive scintillant screen was continuously recorded using a high resolution photon-counting system (HRPCS, Photek Inc., St Leonards on Sea, UK) equipped with a three-stage multichannel plate (MCP) image intensifier. In this system, the gain of the MCP

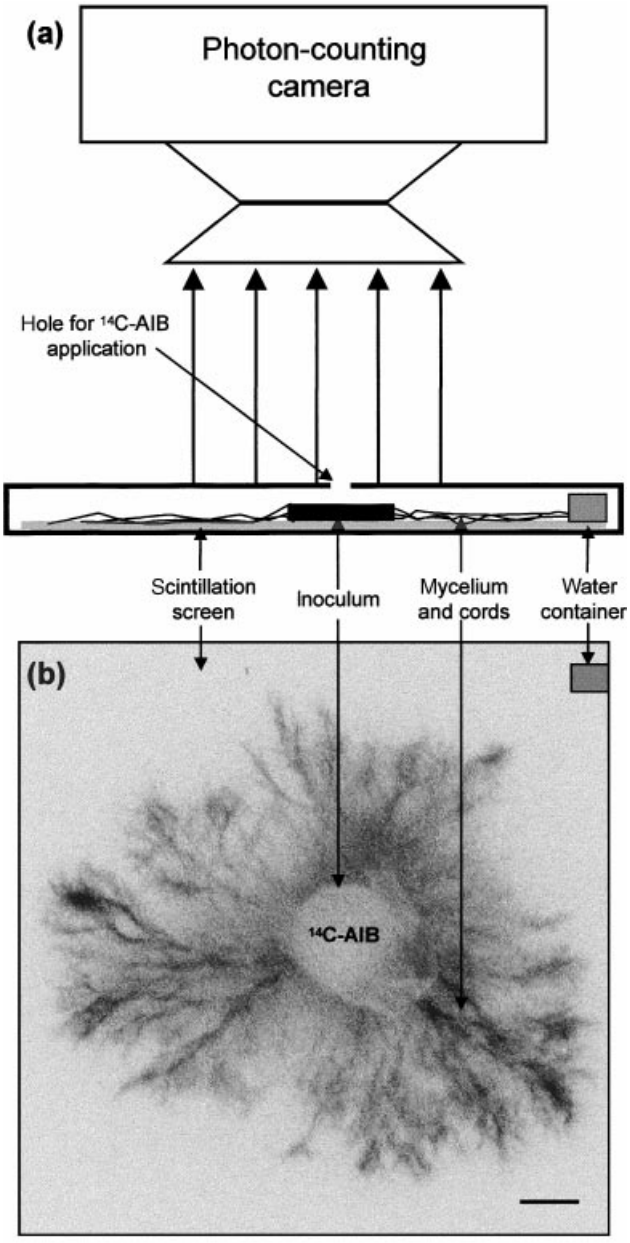

Fig. 1 Typical set-up of a scintillation imaging experiment. (a) A schematic representation of the experimental chamber. *Phanerochaete velutina* was grown from a central inoculum in a sealed square Petri dish chamber over a scintillation screen. ^{14}C-AIB was applied to the inoculum through a central hole. Scintillations from the ^{14}C-AIB were imaged using a photon counting camera. Water was provided in a container to keep the culture at high humidity. (b) A typical image integrated over an 8 h period, for a 14 days culture of *P. velutina*. Bar, 10 mm.

intensifier is set so that every detected photon event on the camera faceplate is discriminated from background noise in the charge coupled device (CCD) array. Normally, MCP intensifiers reduce the spatial resolution of the final image as the signal becomes spread over several pixels on the CCD array, however, in this system the high spatial resolution is maintained by analysing and recording the centre of gravity of the detected image for each photon. With the lenses used here, the nominal (x,y) pixel dimensions were 230×230 μm. Data was output as a sequence of the (x,y) co-ordinates for each detected event, allowing real-time output of data. The sequence file was then analysed, postcapture, to reconstruct images that could be integrated over essentially any defined time interval. Typically images were integrated over either 30 min or 120-min periods and experiments lasted for up to 336 h. Each experiment was repeated at least three times.

Data analysis

To record the rate of outward spread of ^{14}C-AIB photon emissions in growing colonies, the total number of photons was measured in evenly spaced concentric annuli, 12 pixels wide (2.76 mm) round the inoculum starting at a radius of 9 mm. To follow changes along a specific radius, for example when analysing spread along a mycelial cord, data were collected from a series of consecutive areas along the length of the cord.

Fourier techniques were used to determine the frequency of the oscillations in signal from each area and to determine the degree to which the oscillations occurred synchronously across the colony. The data for each area comprised 90–120 samples integrated over 30-min periods. These values were smoothed with a rolling 3 or 5 point averaging filter and any long-term trends eliminated by taking the 2nd difference of each sequence (Diggle, 1990). Visual inspection indicated that this provided a reasonably stationary time-series suitable for Fourier analysis. Each series was padded with zeros to give a total of 256 values, thereby increasing the resolution of the Fourier spectrum (Smith, 1997).

To determine the rate of growth, images integrated over 30 min time intervals were median filtered using a 3×3 box and then thresholded to produce a binary image of the colony morphology as revealed by the distribution of ^{14}C-AIB. If required, the central area of each image containing the inoculum was filled using a hole-fill operation and the area, longest chord and feret diameters were automatically measured. Reflected light images were also collected at intervals during some experiments, however, the contrast achieved between the white mycelium and white scintillation screen made it difficult accurately to delineate the structure of the colony and this approach proved unsuitable for quantitative analysis.

Images were analysed using IFS32 Imaging Software (Photek Inc.) and Lucida 4.0 (Kinetic Imaging, Liverpool, UK), numerical analysis and graphical output used Microsoft Excel (Microsoft Corp.), movie files were edited using Confocal Assistant™ (TC Brelje, University of Minnesota, USA) and Lumiere Video Studio (IMSI) and images for publication were assembled in PhotoShop™ (Adobe Systems, San Jose, CA, USA).

Calibration

To determine the sensitivity and linearity of the photon-counting imaging system, 20 µl droplets of a ^{14}C-AIB dilution series from 0 to 0.925 kBq ^{14}C-AIB were allowed to dry on to the scintillation screen and imaged with identical instrument settings.

To relate the number of photons emitted by the scintillation screen to the amount of ^{14}C present in mycelium in contact with it, the amount of radioactivity in defined regions of each sample, such as a mycelial cord, was measured using liquid-phase scintillation counting in a multichannel β-spectrometer (Beckman LS1801, Beckman Instruments, Inc., CA, USA). Mycelium from different areas of the colony was harvested and placed directly in scintillation vials containing 1 ml of water and 2 ml of liquid scintillation cocktail OptiPhase 'HiSafe'3 (Fisher, Loughborough, UK).

Results

Transport of ^{14}C-AIB in growing mycelium

To test whether ^{14}C-AIB was taken up and how it was distributed within growing colonies of *P. velutina*, movement of ^{14}C-AIB was mapped during the early phase of growth immediately after subculture. The pattern of radioactivity followed the initial growth of the new mycelium as it spread over the scintillation screen (Figs. 2a, S1). Few photons were observed from the region overlaid by the inoculum disc, presumably due to absorption or scattering of light emissions in the agar plug. The mycelium that emerged was labelled and, as the mycelium grew, discrete clusters of hyphae at the colony margin could be readily distinguished, particularly if the integration window was increased from the normal 30-min period. For example, the images shown in Figs 1(a) and 2(a) were integrated over an 8 h period from a continuous sequence lasting 225 h.

The radial growth rate of the colony was determined as either the maximum chord length across the colony or the area of the mycelium, following segmentation of the scintillation images using an intensity threshold (e.g. Fig. 2b). There was little growth over the first 30 h following subculture (Fig. 2c). After this lag period there was an almost linear increase in colony radius for around 50 h at an average rate of 0.20 mm h^{-1}. The rate of radial extension slowly declined after this period and eventually stopped completely after around 120 h (Fig. 2c). For comparison, the average growth rate was 0.24 mm h^{-1} for cultures grown across Petri-dishes without a scintillation screen and with no AIB added (data not shown). Although radial extension ceased, the colony appeared to continue to produce more hyphae, but they were restricted to the region around the inoculum and included many more aerial hyphae.

The total amount of radioactivity present in the mycelium, exported from the inoculum disc, increased simultaneously with colony growth, but with a marked oscillation superimposed on the overall sigmoidal trend (Fig. 2d). The first oscillation was just discernible after approx. 40 h and continued throughout the rest of the time-course with a period of 14.5 ± 1.5 h (n = 54 oscillations from three separate experiments). The amplitude of the oscillation corresponded to approx. 12.5% of the total signal. The pulsing behaviour continued even after radial extension had apparently ceased (Fig. 2d). The distribution of radioactivity in the colony also appeared to change slowly with a longer time constant. To follow these changes in more detail, the signal over concentric rings at 2.76 mm spacing from the centre of the colony was analysed (Fig. 2e).

The pulsatile component was very marked, particularly in the innermost rings, with an amplitude of approx. 17% of the maximum signal. There was little or no detectable shift in the timing of the peaks for oscillations in each concentric ring, suggesting that the oscillations were approximately synchronized across the whole colony within the time-resolution of the integration period used in these measurements (30 min). In addition to these oscillations, the maximum intensity appeared to shift slowly out from the centre through each annulus in turn at a rate of 0.067 mm h^{-1} (Fig. 2f).

The oscillations were not due to cyclical changes in instrument sensitivity, as calibration drops in parallel experiments gave constant signals over extended periods (data not shown). In addition, no spread of radioactivity was observed from control agar discs lacking mycelium (data not shown). Oscillations were not synchronized with changes in temperature, as the temperature recorded within the imaging enclosure remained constant over the imaging period (data not shown), nor with obvious light-triggers as the mycelium was maintained in darkness throughout. Oscillations were not observed in growing colonies of *Serpula lacrymans* imaged under identical conditions (data not shown).

Imaging rapid transport of ^{14}C-AIB in established mycelium

From the first series of experiments, it appeared that the colony sensed the presence of AIB and altered its developmental programme to capitalize on the apparent N-source in the inoculum, even though the added AIB was non-metabolizable. The growth rate slowed after approx. 80 h and the growth pattern was altered. Although it was possible to continue to image the colony for longer periods, it was decided to track ^{14}C-AIB translocation in established colonies over a much shorter time period (40 h) to avoid the additional complications of changing colony development on the interpretation of ^{14}C-AIB redistribution patterns.

When established colonies of *P. velutina* with cords were fed with ^{14}C-AIB applied to the inoculum disc, radioactivity was observed to spread rapidly to the colony margin and to accumulate markedly in the actively growing tips (Figs. 3a,b and

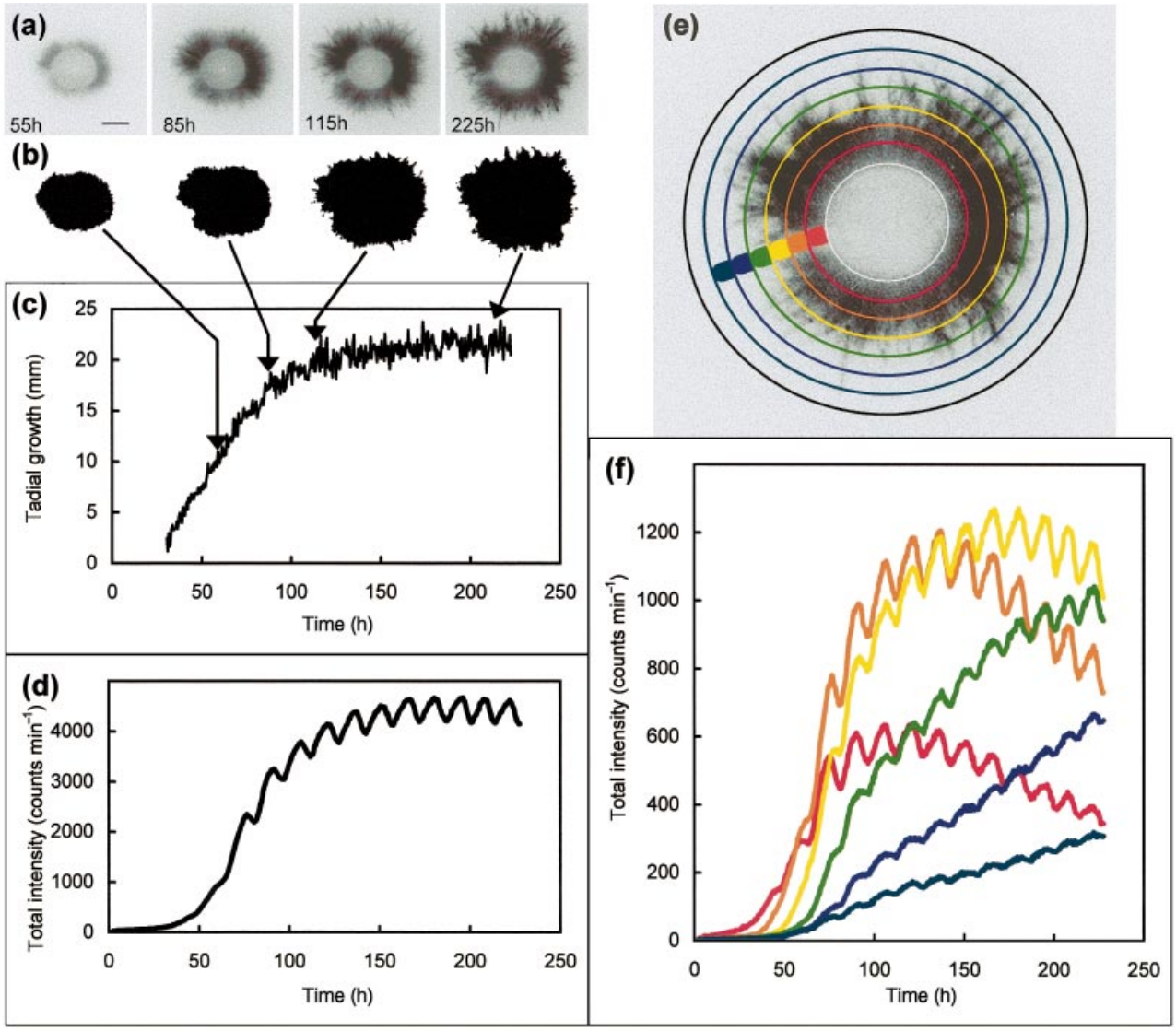

Fig. 2 Transport of ^{14}C-AIB in growing mycelium of *Phanerochaete velutina*. (a) Time-lapse images of ^{14}C-AIB distribution applied to growing mycelium immediately after subculture. Each image was integrated over 8 h. Bar, 10 mm. (b) The colony growth rate was determined by image analysis of binary images segmented from images of the labelled mycelium using a user-defined intensity threshold. (c) A graph showing the radial growth of mycelium estimated from the maximum chord length across binary images following 30 min integration periods over a total of 225 h. (d) A graph showing the time course for the total number of photon counts for the growing mycelium, excluding signal from the central inoculum disc. (e) A schematic diagram showing the arrangement of concentric rings used to trace the radial spread of ^{14}C-AIB during growth. (f) Time course for the total number of photon counts in each annulus shown in (e).

S2). Signal was restricted to mycelium within a few mm of the inoculum for the first 6–7 h and then rapidly spread to the colony margin 30–40 mm distant within the next 1.5–3 h (Fig. 3a). To provide a more detailed understanding of this rapid radial translocation, the total intensity was measured for successive regions on the selected cords shown in Fig. 3(b). The flux was visualized as contour plots of intensities from these areas for three of the longer cords (Fig. 3c). In all three cords, the signal appeared in the first region, centred approx. 8 mm from the inoculum, within 2–3 h. During the rapid phase of translocation, starting around 6.5 h, the moving front of radioactivity traversed up to 30 mm in approx. 1.5 h (20 mm h^{-1}). Similar results were observed for other cords in this colony and in two other colonies analysed.

The signal continued to increase markedly at the colony margin and, to a lesser extent, in the intervening cords following this rapid surge. The increase was not linear, but took the form of a series of discrete steps in the terminal web of growing hyphae at the tip of each cord, accompanied by a series of oscillations within the cords themselves (Fig. 3d). At the

New Phytologist

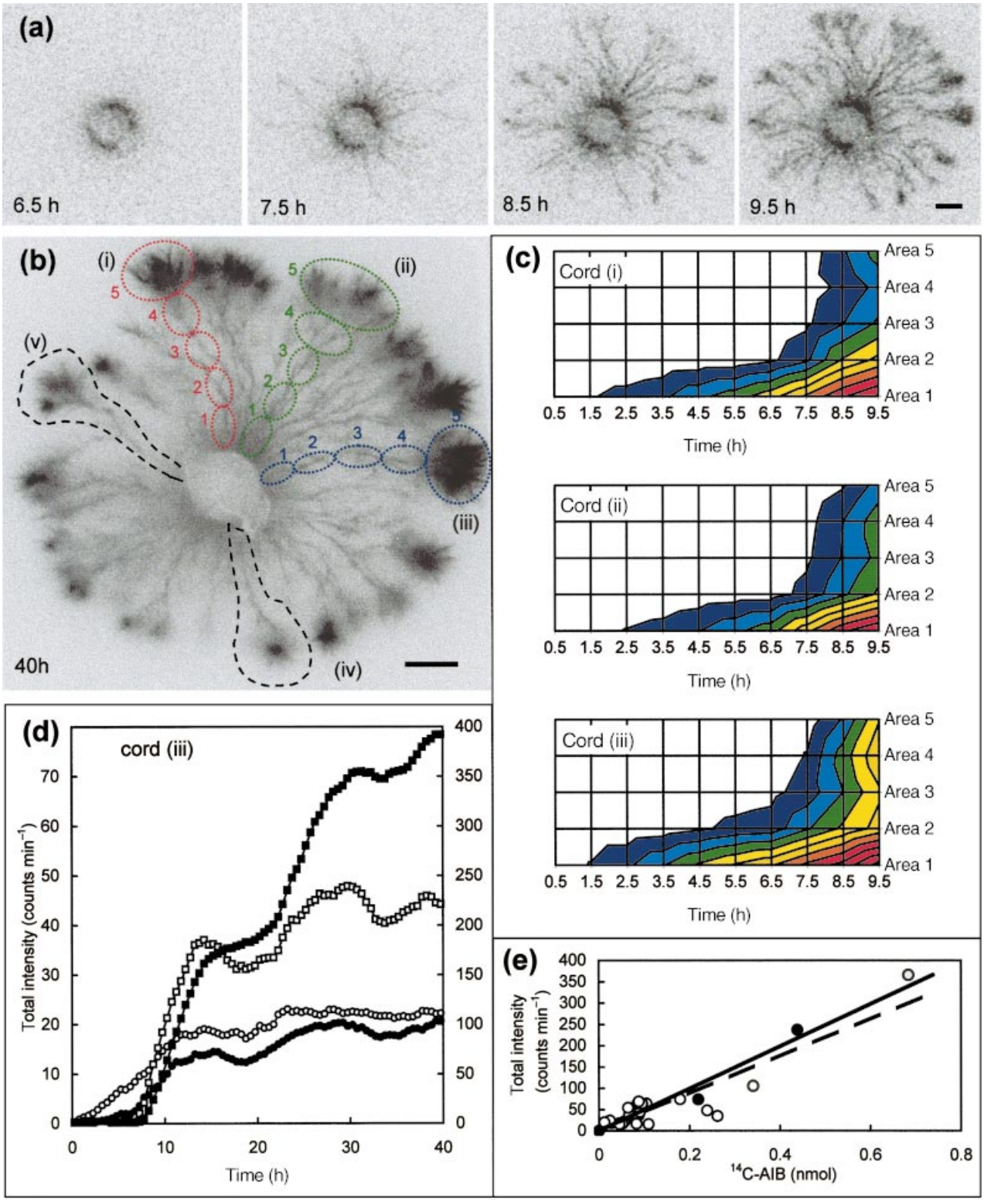

Fig. 3 Rapid transport of ^{14}C-AIB in established mycelium and cords. (a) Time-lapse imaging of ^{14}C-AIB translocation following application of the radioactive amino acid to the original inoculum disc of a 3-wk-old-culture. Each image was integrated over 1 h. Bar, 10 mm. Rapid transport of ^{14}C-AIB is visible as a spread of signal to the colony margin over a few hours. (b) Schematic representation of the cords and areas along each cord used for subsequent analyses shown overlaid on an image integrated for 8 h, 40 h after the label was applied. Substantial accumulation of ^{14}C-AIB is apparent at the hyphal webs at the end of each cord by this time. Five different cords used for data analysis were marked from (i) to (v). The signal from each cord was analysed from 5 adjacent areas. Bar, 10 mm. (c) Colour-coded contour plots showing rapid spread of

Table 1 Transport of ^{14}C-AIB in established colonies of *Phanerochaete velutina*

		Cord length (mm)	^{14}C-AIB accumulation at tips (pmol pulse^{-1})	Average ^{14}C-AIB per cord (pmol)	Maximum accumulation rate (pmol h^{-1})	Estimated minimum transport rate required (mm h^{-1})	Pulse propagation rate (mm h^{-1})	Estimated mobile fraction (%)
Colony 1	Cord (i)	43	212	131	30.0	13.9	37.4	37.0
	Cord (ii)	42	208	294	30.9	5.9	18.3	32.5
	Cord (iii)	43	416	240	51.5	14.9	23.4	63.6
	Cord (iv)	33	55	109	7.6	3.3	10.7	30.9
	Cord (v)	34	118	132	14.7	6.1	19.1	31.8
Colony 2	Cord (i)	28	69	212	6.1	1.8	9.5	19.2
	Cord (ii)	35	280	310	30.6	6.3	23.6	26.9
	Cord (iii)	28	95	170	13.3	3.1	16.6	18.9
	Cord (iv)	33	227	429	25.3	3.5	24.9	14.1
Colony 3	Cord (i)	38	82	346	10.8	1.8	16.8	10.7
	Cord (ii)	40	43	127	4.9	2.7	34.4	7.9
	Cord (iii)	38	162	189	18.9	6.5	13.6	48.0
	Cord (iv)	48	321	869	31.6	3.5	51.8	6.9
	Cord (v)	40	28	86	4.6	2.6	21.1	12.3

colony margin, there was a period of substantial ^{14}C-AIB accumulation lasting 6–8 h, followed by a relatively stable plateau lasting a further 4–6 h. By contrast, the signal along the intervening cord settled down to a regular oscillation about a much lower overall level with a similar overall period (Note in Fig. 3d the signal from the cords and margin are expressed on different scales).

To quantify the amount of ^{14}C-AIB accumulated from such images required a calibration to convert from photons detected to the amount of ^{14}C-AIB present in the mycelium. A near linear calibration (r^2 = 0.959) was found for droplets of ^{14}C-AIB standards dried down on to the scintillation screen with a gradient of 496 photons min^{-1} nmol^{-1} ^{14}C-AIB (Fig. 3e). In a more realistic calibration, the relationship between photons detected *in situ* from ^{14}C-AIB in selected regions of the mycelium and the subsequent amount of ^{14}C-AIB detected by conventional liquid-phase scintillation counting was determined (Fig. 3e). The total recovery of radioactivity was 94 ± 6% (n = 7) for the initial inoculum disc and all regions of the mycelium. The regression against photon counts for the *in situ* calibration was only slightly lower than the calibration against ^{14}C-AIB standards (440 photons min^{-1} nmol^{-1} ^{14}C-AIB), however, there was a much higher variance in the data (r^2 = 0.812) (Fig. 3e). Using the *in situ* calibration, the amount of ^{14}C-AIB appearing in the hyphal net at the tip of each cord ranged over more than an order of magnitude from 28 to 416 pmoles during each pulse, and the maximum rate of net transfer ranged from 4.6 to 51.5 pmol h^{-1} (Table 1). In general, higher levels of ^{14}C-AIB accumulation and slightly faster rates of net transfer were associated with longer cords subtending a larger mass of hyphae (Table 1).

The observation of an oscillation in the cords but a step-wise increase at the margin was highly suggestive of a series of pulses delivering ^{14}C-AIB through the cord to the growing mycelium. It was therefore of interest to determine whether there was any evidence for a wave of radioactivity spreading out from the inoculum, and, if so, to determine the maximum speed of its propagation.

The frequency of the oscillations was determined from Fourier analysis of the time-series derived from a series of areas along four or five selected cords for each colony. The areas used for three of the cords are shown in Fig. 3(b). The second difference of each time series was used to remove the long-term trends in each series (Fig. 4a). In all cases, the Fourier spectra of the transformed data were dominated by a major peak with a Fourier frequency of 10 or 11 corresponding to a

Fig. 3 *(continued)* ^{14}C-AIB for cords (i–iii). Blue represents low signals and red higher signals. Each plot has been scaled relative to the maximum signal in area 1 after 9.5 h. In all three cases there was a surge of signal to the colony margin between 6.5 and 8.5 h. (d) A graph showing the time-course for ^{14}C-AIB movement in cord (iii). Following the initial surge to the margin, oscillations were observed for areas along the cord and a more substantial, step-wise increase at the periphery (note area 5 is plotted on the right hand scale). Area 1, open circles; area 2, closed circles; area 4, open squares; area 5, closed sqaures. Data from area 3 has been excluded for clarity. (e) Calibration curve of the camera system. The number of photon counts min^{-1} was plotted against either the amount of ^{14}C-AIB dried down from droplets onto the scintillation screen (closed circles) or the amount of ^{14}C-AIB determined by liquid scintillation counting of mycelia harvested following the imaging experiment (open circles). The linear regression (solid line) was 496 photons min^{-1} nmol ^{14}C-AIB for the standards and 440 photons min^{-1} nmol ^{14}C-AIB for the cords (dashed line).

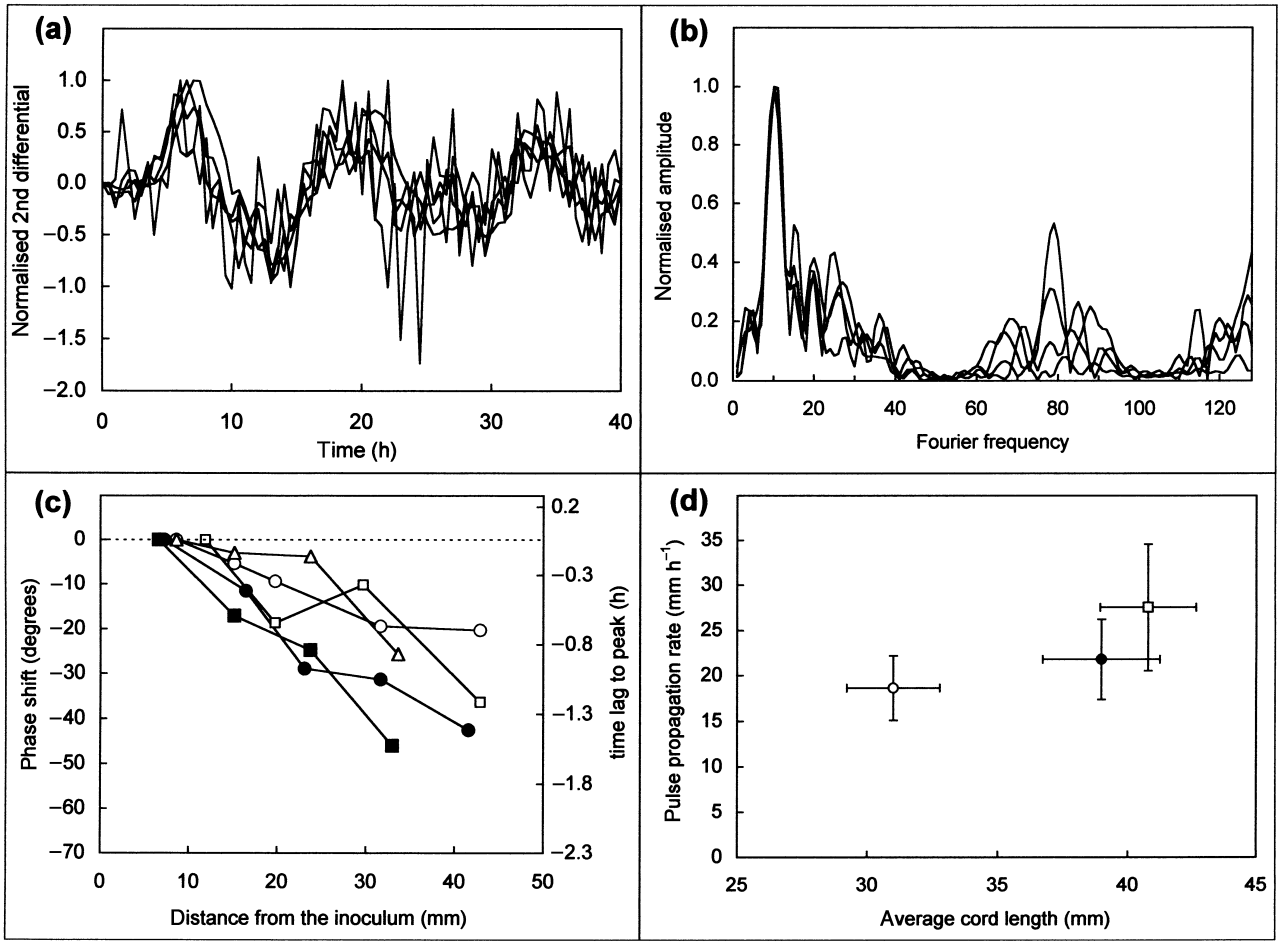

Fig. 4 Fourier analysis of the pulsatile component of ^{14}C-AIB translocation. (a) Long-term trends in the signal from each area along a cord were removed by taking the 2nd difference of the time-series. Data, normalized to the first peak in the series to accommodate the difference in amplitude for different regions, are overlaid for each area from cord (iii). (b) Fourier spectra for the data shown in (a) after padding with zeros to increase the spectral resolution to 128 Fourier frequencies. Traces have been normalized to the dominant frequency for comparison. The main peak corresponds to a time period of 11.63 h. (c) Phase shifts for the dominant Fourier frequency with distance along the cord for five different cords in the same colony. There was a trend in the phase difference of 20–50° corresponding to a lag of 0.5–1.5 h from near the inoculum to the colony margin. (d) Average propagation rate along the cord of the peak signal for three different colonies based on analysis of 4–5 cords per colony. The average propagation rate of the pulse was around 23 mm h^{-1}, with a slight trend towards faster rates in longer cords.

period of 12.80–11.64 h, depending on the experiment (Fig. 4b). Additional peaks with periods clustered between 3.6 and 6 h and 1.4–2 h were also present, but with lower amplitude and with greater variability between experiments. There was a slight, but consistent shift in the phase of the dominant frequency of approx. 20–50° with the distance along each cord corresponding to a time lag of 0.5–1.5 h between the peak of the oscillation near the inoculum and the peak arriving at the colony margin (Fig. 4c). Taking into account the length of each cord, this corresponds to an average velocity for propagation of the pulse ranging from 18 mm h^{-1} to 27 mm h^{-1} from individual colonies (Fig. 4e), although the variation between different cords in the same colony was more marked (9.5–51.8 mm h^{-1}; Table 1). There was a tendency for faster propagation rates to be associated with longer cords (Fig. 4d; Table 1).

Discussion

Photon-counting scintillation imaging can be used to map ^{14}C-amino acid translocation in intact, living mycelia

Movement of ^{14}C-AIB in mycelia of *P. velutina* was imaged under a variety of experimental conditions with a practical time resolution of 10–30 min and continuous sampling for periods in excess of 300 h. The lowest detectable level of ^{14}C-AIB for a 1 h integration period was approx. 100 fmol

^{14}C-AIB mm^{-2} h^{-1} (5.4 fmol pixel^{-1} h^{-1}), with a signal to background ratio of better than 2 : 1. The notional pixel spacing for these experiments was 230 μm in both *x* and *y*, however, the actual spatial resolution achieved was affected by the exponential spread of radioactivity away from the ^{14}C-AIB in the hyphae and the low signal-to-noise (S : N) ratio possible with a weak emitter such as ^{14}C. For example, the signal integrated for 1 h from each of the major cords 9.5 h after loading shown in Fig. 3(a) corresponds to approx. 26–60 pmol ^{14}C-AIB cord^{-1} (approx. 200–500 fmol mm^{-2}). Increasing the integration time to 8 h after the level of ^{14}C-AIB had increased 10-fold was sufficient to reveal the fine meshwork of hyphae between these thicker cords (e.g. Fig. 3b). Although these first results are extremely encouraging, we also believe that it should be relatively straightforward to increase the sensitivity of this technique further by: cooling the MCP and CCD array to reduce background thermal noise; increasing the detection area of the MCP; improving the efficiency of light capture with faster lenses and optimized optics; and selecting scintillation screens with enhanced sensitivity for weak emitters. With respect to this latter point, preliminary investigation with the Kodak BioMax TranScreen LE intensifying screen gave an increase in signal by a factor of at least 4–5. Taken together, these factors are likely to routinely give a 10-fold increase in sensitivity and a 100-fold increase is possible, giving a detection limit of 1 fmol mm^{-2}.

To our knowledge, three other methods have been used to map ^{14}C movement in living fungal colonies. Jennings and co-workers used high-efficiency Geiger-Müller tubes to make some of the first *in situ* transport velocity measurements (Brownlee & Jennings, 1982). This approach provides high sensitivity, but very low overall spatial resolution. Olsson and coworkers pioneered *in vivo* imaging of radioisotopes using a β-scanner (e.g. Timonen *et al.*, 1997; Olsson & Gray, 1998), which provides a similar practical sampling rate to the system described here (roughly 1 h based on the scanned area and integration time used) and similar sensitivity (minimum detectable level 114.7 fmol AIB mm^{-2}). The spatial resolution used for ^{14}C imaging with the β-scanner (0.78 × 3 mm pixel dimensions; Olsson & Gray, 1998) was somewhat lower than the method described here. More recently, Lindahl *et al.* (1999, 2001) have used an electronic autoradiography system to image phosphorus transfer between mycelium of a wood decomposing and an ectomycorrhizal fungus, and Leake *et al.* (2001) applied this method to measuring ^{14}C-fluxes from *Pinus sylvestris* seedlings to mycelia of its mycorrhizal partner, *Paxillus involutus*. This system is based on detecting ionizing radiation from β-particles using an array of high-density avalanche chambers. The nominal pixel spacing is around 1 mm and our estimate of the minimum detection sensitivity is around 10 fmol mm^{-2}. A major advantage of both the β-scanner and the electronic autoradiography system is that isotope translocation can be visualized in colonies grown across a range of substrates, including agar or even soil-based microcosms, rather than limited to fungi that will grow across a scintillation screen. A major advantage of the system described here is the increase in spatial resolution at comparable sensitivity.

For quantitative work, tracking the weak emissions from ^{14}C is quite challenging whichever system is used. The maximum energy from ^{14}C is 0.156 MeV, which translates into a maximum penetration depth of 280 μm through water. The average energy is expected to be about one third of this, giving a penetration depth of around 100 μm. There is likely to be further attenuation when the ^{14}C is present within the mycelium due to absorption by the wall components and hyphal contents. In addition, absorption, refraction and scattering of the photons emitted from the scintillation screen as they pass back through the mycelium will further reduce the signal that can be detected. An extreme example of this problem is the absence of signal from the inoculum plug even though this was where the ^{14}C-AIB was loaded. For the age of colonies studied here, we estimate that the sum of these effects is approx. a 10% loss in signal, witnessed in the difference in calibration curves between ^{14}C-AIB standards and ^{14}C-AIB measured *in situ* within the mycelium. Within this general trend, the spread of the *in situ* calibration data might reflect more pronounced effects for some regions, such as well developed cords, in comparison with fine hyphae at the colony margin. For comparison, Leake *et al.* (2001) found an approximate 1.5-fold reduction in detectable β-emissions from roots compared to mycorrhizal mycelium.

Development in *P. velutina* is affected by AIB

In common with many other species (Watkinson, 1984a; Elliott & Watkinson, 1989; Lilly *et al.*, 1990), *P. velutina* rapidly took up AIB and carried it to growing hyphae at the colony margin. After approx. 80 h of growth, AIB triggered a shift from radial expansion to more subapical branching that resulted in formation of a dense cushion around the inoculum. Similar changes in colony development, most pronounced in the absence of carbon and nitrogen nutrients, have been reported for 16 other basidiomycete and ascomycete fungi grown on agar when AIB was uniformly supplied at high (0.1–1 M) concentration (Elliott & Watkinson, 1989; Watkinson, 1999). This change in growth pattern is normally triggered by an encounter with a localized resource or the stochastic arrival of a new resource, such as wood block. The increase in hyphal density would typically result in increased exploitation of such a patchy resource (Ritz & Crawford, 1996; Donnelly & Boddy, 1998; Boddy, 1999). AIB is clearly able to induce such responses even though it is not metabolized. The effects of AIB are long-lived as AIB remains in the mycelium for periods up to several months (the longest period tested) and can inhibit hyphal extension at a distance from the point of application (Dobson *et al.*, 1993). The sensitivity of different fungi to AIB is variable and in the case of *Schizophyllum commune* no effect was observed on colony morphology for

AIB at concentrations around 10 mM even though the AIB was taken up and translocated (Lilly *et al.*, 1990).

In comparison to other fungi, *P. velutina* in the present experiments seems to be remarkably sensitive to AIB. If the amount of ^{14}C-AIB added to the inoculum were evenly distributed, it would be equivalent to a concentration of approx. 22.5 μM, a concentration considerably lower than that used in other experiments. The enhanced sensitivity of *P. velutina* to AIB may also reflect the limited availability of other amino acids when an inoculum disc is used as the sole nutrient source. In systems grown on agar, AIB inhibition was counteracted by nutrients in the medium (Elliot & Watkinson, 1989). From this result we conclude that some caution is required when interpreting experiments that use ^{14}C-AIB as an amino-acid analogue, particularly in long-term (> 6 d) experiments, as the distribution patterns observed may well incorporate physiological and developmental responses of the system. The effects may also change over time and become more pronounced if other utilisable nutrients are progressively removed by metabolism and the AIB comes to represent a larger fraction of the intracellular pool of amino acids.

Cords support rapid amino acid fluxes

Translocation in cords and mycelium of large fungal colonies is known to occur at rates faster than diffusion and the data presented here confirm this for amino-acid translocation in *P. velutina*. The velocity of amino acid movement in the cords was estimated by analysing the data in two different ways. In the first analysis, the rate of spread of the radioactive front was measured. After a short lag following loading, the initial spread of radioactivity was observed mainly in the cords, reaching the colony margin within a 1–2-h period. Depending on the length of the cord, the rate of movement of the front was around 20 mm h^{-1} (Fig. 3c). Although the rapid movement could be clearly seen, it was difficult to define precisely where the leading edge of the spreading wave was located as the signal was low and noisy. The second approach used Fourier analysis to interrogate the entire time-sequence rather than just the initial spread. This approach took advantage of the pulsatile nature of amino acid movement in this fungus to determine the rate of propagation of the pulse towards the margins. The average propagation rates for pulses along cords from three different colonies were also clustered around 23 mm h^{-1} (Fig. 4d), although this to some extent hid considerable variability within individual cords, where the propagation rate could be as fast as 50 mm h^{-1} (Table 1). There was a slight trend for increased propagation rates with increasing cord length that probably reflected increasing cord maturity. Within a single colony, there appeared to be competition between different cords, with the most active translocating an order of magnitude more ^{14}C-AIB than their shorter, less well developed counterparts at a correspondingly faster net rate (Table 1). For comparison, using the experimentally measured diffusion coefficient of 3.6×10^{-6} cm^2 s^{-1} in agar determined by Olsson & Gray (1998), it would take a minimum of approx. 174 h for ^{14}C-AIB to diffuse 30 mm. The rates of transport observed here are thus significantly faster than diffusion.

The translocation velocities reported here were considerably faster than the maximum estimate of ^{14}C-AIB movement of 1.8 mm h^{-1} for *Pleurotus ostreatus* and *Schizophyllum commune* (Olsson & Gray, 1998), but lower than velocities reported for ^{14}C-aspartic acid and ^{32}P-phosphate in cords of *Serpula lacrymans* (Brownlee & Jennings, 1982).

It is instructive to consider what mass flow of ^{14}C-AIB would be required in each cord to achieve the delivery rate observed at the margin during each pulse if all the ^{14}C-AIB in the cord were free to move. Using the integrated signal along the cord as a measure of the amount of ^{14}C-AIB present in the cord, the minimum mass flow required ranges from 1.8 to 14.9 mm h^{-1} (Table 1). These values are considerably lower than the rates of movement observed for either the initial spread ^{14}C-AIB front or the propagation rate of the pulse. If the latter two parameters indeed reflect the speed of movement along the transport pathway, the difference between these values and the estimate from the minimum mass flow of ^{14}C-AIB required in the cord, could be attributed to movement of only a relatively small proportion of the ^{14}C-AIB. Based on the ratio of the pulse propagation rate to the calculated turnover rate of ^{14}C-AIB would give values of 6.9–63.9% of the ^{14}C-AIB being mobile in each cord. It is notable that the amplitude of the oscillation is also in the region of 20% of the signal present.

Amino acid translocation in *P. velutina* has a pulsatile component

The pulses in ^{14}C-AIB movement are evidence for a rhythmic process in *P. velutina* mycelium that has not been previously reported. Electrical signals, resembling nerve action potentials, have been found in cords of similar fungi, although not in the context of amino acid translocation. These electrical signals have a much higher and more variable frequency than the pulses reported here (Olsson, 1995).

When ^{14}C-AIB translocation was followed in established mycelium, there was good evidence for the most active cords that most if not all of the material in the pulse was delivered to the colony margin and resulted in a net stepwise increase in signal from this region. The pulsatile signal observed for the growing colony is less readily explained. Pulsing was observed to continue even when AIB had effectively arrested further radial extension, but was not accompanied by accumulation at the colony margin. We can offer two explanations. First, there may be cyclical changes in the fungal structure or local distribution of ^{14}C-AIB that alter the efficiency with which photons are generated or detected. For example, rhythmical movement of ^{14}C-AIB into hyphae further away from the screen perhaps within the centre of a cord or aerial hyphae

might modulate the number of β-particles reaching the screen. Alternatively, changes in the turgor and water content of the mycelium might affect its optical properties and therefore modulate the detection efficiency of photons emitted from the underlying screen. In either case, the pulses still reflect interesting physiological processes taking place within the mycelium, but the apparent impact on amino-acid translocation *per se* might be misleading. A second explanation is that the pulsing reflects operation of a basipetal flux back to the central inoculum. It is clear that little or no signal can be detected from the central inoculum as much of its volume lies further away from the screen than the maximum penetration depth of ^{14}C emissions and it is opaque, effectively blocking detection of any emitted photons. Under these conditions, we would predict that ^{14}C-AIB returning to the inoculum would temporarily become invisible and lead to a decrease in net signal. This observation would be consistent with the idea that nutrients effectively cycle through the mycelium from loading sites and are tapped off as required at different sinks (Wells *et al.*, 1998b; Boddy, 1999; Lindahl *et al.*, 2001). It does not seem that such behaviour is a universal feature of foraging saprotrophs as we have not observed similar pulsing in *S. lacrymans* grown under similar conditions (data not shown). One intriguing possibility is that pulsing provides additional signalling information in fungi with a long-range foraging strategy, where encounters with localized new resources stimulate developmental responses at relatively distant parts of the mycelium. There are a limited number of precedents for such a hypothesis. Olsson (1995, 1999) found a pulsed electrical potential in cords that responded to contact with a nutrient source by a change in frequency and suggested that this could represent a foraging signal. The frequency of these action-potential like pulses was orders of magnitude higher than the frequency of ^{14}C-AIB movement found here. Within a more comparable time frame, pulses in extracellular cAMP are well established as part of the signalling system leading to aggregation of *Dictyostelium discoideum* amoebae in response to nutrient depletion (Gerisch, 1987; Dormann *et al.*, 2000). Whilst the observed pulsing has to be incorporated into any model describing nutrient translocation in *P. velutina*, there is an additional intriguing possibility that coordinated responses of *P. velutina* following contact with a fresh resource are mediated by changes in frequency or amplitude of a pulsed long distance signal travelling in the mycelium.

Acknowledgements

We are grateful to Profs. A. E. Ashford and L. Boddy for generously sharing with us their technique and expertise. Our colleagues Drs M. Dewey and S. Gurr kindly read and commented on the manuscript. Dr M. Knight loaned us the photon counting camera. The work was supported by grant no. GR3/12946 from the Natural Environment Research Council of Great Britain.

Supplementary material

The following video material is available from http://www.blackwell-science.com/products/journals/suppmat/NPH/NPH288/NPH288sm.htm

Fig. S1 Distribution of ^{14}C-AIB during growth of *Phanerochaete velutina*. The video spans 160 h at 4 h intervals following loading of the central inoculum with 44 nmoles ^{14}C-AIB immediately after subculture. After approx. 24 h, the fungus begins to grow out from the agar plug. Continuous pulsing is apparent across the colony with a period of around 12 h. Images are shown at the original pixel spacing, the colony diameter is approx. 40 mm.

Fig. S2 Rapid ^{14}C-AIB movement in cords of *Phanerochaete velutina*. The video shows an animated sequence of 40 images, each integrated over 1 h, following addition of 44 nmoles of ^{14}C-AIB to the central inoculum plug of a 20-d-old-colony. Rapid movement of ^{14}C-AIB to the colony margin is apparent within the first few hours and is followed by a series of pulses. The colony continues to grow radially during the experiment. Images were subsampled by a factor of 2 in (x,y) to reduce download times. The colony diameter is approximately 90 mm.

References

Amir R, Steudle E, Levanon D, Hadar Y, Chet I. 1995. Turgor changes in *Morchella esculenta* during translocation and sclerotial formation. *Experimental Mycology* **19**: 129–136.

Arnebrandt K, Ek H, Finlay RD, Soderstrom B. 1993. Nitrogen translocation between *Alnus glutinosa* (L.) Gaertn. Seedlings infected with *Frankia* sp. and *Pinus contorta* Doug. Ex Loud seedlings connected by a common ectomycorrhizal mycelium. *New Phytologist* **130**: 231–242.

Boddy L. 1993. Saprotrophic cord forming fungi: warfare strategies and other ecological aspects. *Mycological Research* **94**: 641–655.

Boddy L. 1999. Saprotrophic cord-forming fungi: meeting the challenge of heterogeneous environments. *Mycologia* **91**: 13–32.

Boddy L, Watkinson SC. 1995. Wood decomposition, higher fungi, and their role in nutrient distribution. *Canadian Journal of Botany* **73**: S1377–S1383.

Boddy L, Wells JM, Culshaw C, Donnelly D. 1999. Fractal analysis in studies of mycelium in soil. *Geoderma* **88**: 301–308.

Brownlee C, Jennings DH. 1982. Long distance translocation in *Serpula lacrymans*. Velocity estimates and the continuous monitoring of induced perturbations. *Transactions of the British Mycological Society* **79**: 143–148.

Cairney JWG. 1992. Translocation of solutes in ectomycorrhizal and saprotrophic rhizomorphs. *Mycological Research* **96**: 135–141.

Cairney JWG, Jennings DH, Veltkamp CJ. 1989. A scanning electron microscope study of the internal structure of mature linear mycelial organs of four basidiomycete species. *Canadian Journal of Botany* **67**: 2266–2271.

Cole L, Orlovich DA, Ashford AE. 1998. Structure, function and motility of vacuoles in filamentous fungi. *Fungal Genetics and Biology* **24**: 86–100.

Cromack K, Caldwell BA. 1992. The role of fungi in litter decomposition and nutrient cycling. In: Carroll GC, Wicklow DT, eds. *The fungal community: its organization and role in the ecosystem, 2nd edn*. New York, USA: Marcel Dekker, 653–668.

Diggle PJ. 1990. *Time series. A biostatistical introduction. Oxford statistical science series*. Copas JB, Dawid AP, Eagleson GK, Pierce DA, eds. Oxford, UK: Clarendon Press.

Dobson J, Power JM, Singh J, Watkinson SC. 1993. The effectiveness of 2-aminoisobutyric acid as a translocatable fungistatic agent for the remedial treatment of dry rot caused by *Serpula lacrymans* in buildings. *International Biodeterioration and Biodegradation* **31**: 129–141.

Donnelly DP, Boddy L. 1998. Developmental and morphological responses of mycelial systems of *Stropharia caerulea* and *Phanerochaete velutina* to soil nutrient enrichment. *New Phytologist* **138**: 519–531.

Dormann D, Vasiev B, Weijer CJ. 2000. The control of chemotactic cell movement during *Dictyostelium* morphogenesis. *Philosophical Transactions of the Royal Society of London Series B-Biological Sciences* **355**: 983–991.

Ek H, Andersson S, Soderstrom B. 1996. Carbon and nitrogen flow in silver birch and Norway spruce connected by a common mycorrhizal mycelium. *Mycorrhiza* **6**: 465–467.

Elliott ME, Watkinson SC. 1989. The effect of 2-aminoisobutyric acid on wood decay and wood spoilage fungi. *International Biodeterioration and Biodegradation* **25**: 335–371.

Gerisch C. 1987. Cyclic AMP and other signals controlling cell development and differentiation in *Dictyostelium*. *Annual Review of Biochemistry* **56**: 853–879.

Granlund HI, Jennings DH, Thompson W. 1985. Translocation of solutes along rhizomorphs of *Armillaria mellea*. *Transactions of the British Mycological Society* **84**: 111–119.

Griffin DH. 1994. *Fungal physiology, 2nd edn*. New York, USA: Wiley-Liss.

Harley JH, Smith SE. 1983. *Mycorrhizal symbiosis*. London, UK: Academic Press.

Jennings DH. 1987. The translocation of solutes in fungi. *Biological Reviews* **62**: 215–243.

Jennings DH. 1994. Translocation in mycelia. In: Wessels JGH, Meinhardt H, eds. *The mycota 1: growth, differentiation and sexuality*. Berlin, Germany: Springer-Verlag, 163–173.

Jennings L, Watkinson SC. 1982. The structure and development of mycelial strands in *Serpula lacrymans*. *Transactions of the British Mycological Society* **78**: 465–474.

Kim KW, Roon RJ. 1982. Transport and metabolic effects of alpha-aminoisobutyric acid in *Saccharomyces cerevisiae*. *Biochimica et Biophysica Acta* **719**: 356–362.

Kitamoto K, Yoshizawa K, Ohsumi Y, Anraku Y. 1988. Dynamic aspects of vacuolar and cytosolic amino acid pools of *Saccharomyces cerevisiae*. *Journal of Bacteriology* **170**: 2683–2686.

Klionsky DT, Ohsumi Y. 1999. Vacuolar import of proteins and organelles from the cytoplasm. *Annual Reviews of Cell and Developmental Biology* **15**: 1–32.

Leake JR, Donnelly DP, Saunders EM, Boddy L, Read DJ. 2001. Rates and quantities of carbon flux to ectomycorrhizal mycelium following ^{14}C pulse labeling of *Pinus sylvestris* seedlings: effects of litter patches and interaction with a wood-decomposer fungus. *Tree Physiology* **21**: 71–82.

Lilly WW, Higgins SM, Wallweber GJ. 1990. Uptake and translocation of 2-aminoisobutyric acid by *Schizophyllum commune*. *Experimental Mycology* **14**: 169–177.

Lindahl B, Finlay R, Olsson S. 2001. Simultaneous, bi-directional translocation of ^{32}P and ^{33}P between wood blocks connected by mycelial cords of *Hypholoma fasciculare*. *New Phytologist* **150**: 189–194.

Lindahl B, Stenlid J, Olsson S, Finlay R. 1999. Translocation of ^{32}P between interacting mycelia of a wood-decomposing fungus and ectomycorrhizal fungi in microcosm systems. *New Phytologist* **144**: 183–193.

Miller RM, Lodge DJ. 1997. Fungal responses to disturbance: agriculture and forestry. In: Wicklow DT, Soderstrom B, Esser K, Lemke PA, eds. *Environmental relationships. The Mycota IV*. Berlin, Germany: Springer-Verlag.

Ogilvie-Villa S, DeBusk RM, DeBusk AG. 1981. Characterisation of 2-aminoisobutyric acid transport in *Neurospora crassa*. *Journal of Bacteriology* **147**: 944–948.

Ohsumi Y, Anraku Y. 1981. Active transport of basic amino acids is driven by a proton motive force in vacuolar membrane vesicles of *Saccharomyces cerevisiae*. *Journal of Biological Chemistry* **256**: 2079–2082.

Olsson S. 1995. Action potential-like activity found in fungal mycelia is sensitive to stimulation. *Naturwissenschaften* **82**: 30–31.

Olsson S. 1999. Nutrient translocation and electrical signalling in mycelia. In: Gow NAR, Robson GD, Gadd GM, eds. *The fungal colony*. Cambridge, UK: Cambridge University Press, 25–48.

Olsson S, Gray SN. 1998. Patterns and dynamics of ^{32}P-phosphate and labelled 2-aminoisobutyric acid (^{14}C-AIB) translocation in intact basidiomycete mycelia. *FEMS Microbiology Ecology* **26**: 109–120.

Perez-Moreno J, Read DJ. 2000. Mobilisation and transfer of nutrients from litter to tree seedlings via the vegetative mycelium of ectomycorrhizal plants. *New Phytologist* **145**: 301–309.

Ritz K, Crawford JW. 1996. Colony development in nutritionally heterogeneous environments. In: Gow NAR, Robson GD, Gadd GM, eds. *The fungal colony*. Cambridge, UK: Cambridge University Press, 49–75.

Seiler S, Plamann M, Schliwa M. 1999. Kinesin and dynein mutants provide novel insights into the roles of vesicle traffic during cell morphogensis in *Neurospora*. *Current Biology* **9**: 779–785.

Shepherd VA, Orlovich DA, Ashford AE. 1993. Cell-to-cell transport via motile tubules in growing hyphae of a fungus. *Journal of Cell Science* **105**: 1173–1178.

Smith SW. 1997. *The scientist and engineer's guide to digital signal processing*. california, usa: Technical Publishing.

Steinberg G. 1998. Organelle transport and molecular motors in fungi. *Fungal Genetics and Biology* **24**: 161–177.

Timonen S, Finlay RD, Olsson S, Soderstrom B. 1997. Dynamics of phosphorus translocation in intact ectomycorrhizal systems: non-destructive monitoring using a β-scanner. *FEMS Microbiology Ecology* **19**: 171–180.

Venables CE, Watkinson SC. 1989. Medium-induced changes in patterns of free and combined amino acids in mycelium of *Serpula lacrymans*. *Mycological Research* **92**: 273–277.

Watkinson SC. 1984a. Inhibition of growth and development of *Serpula lacrymans* by the non-metabolised amino acid analogue 2-aminoisobutyric acid. *FEMS Microbiology Letters* **24**: 247–250.

Watkinson SC. 1984b. Morphogenesis of the Serpula lacrymans colony in relation to its function in nature. In: Jennings DH, Rayner ADM, eds. *The ecology and physiology of the fungal mycelium*. Cambridge, UK: Cambridge University Press, 165–184.

Watkinson SC. 1999. Metabolism and hyphal differentiation in large basidiomycete colonies. In: Gow NAR, Robson GD, Gadd GM, eds. *The fungal colony*. UK. Cambridge, UK: Cambridge University Press, 127–157.

Watkinson SC, Davison EM, Bramah J. 1981. The effect of nitrogen availability on growth and cellulolysis by *Serpula lacrymans*. *New Phytologist* **89**: 295–305.

Weiss RL. 1973. Intracellular localisation of ornithine and arginine pools in *Neurospora*. *Journal of Biological Chemistry* **248**: 5409–5413.

Wells JM, Boddy L. 1990. Wood decay, and phosphorous and fungal biomass allocation, in mycelial cord systems. *New Phytologist* **116**: 285–295.

Wells JM, Boddy L, Donnelly DP. 1998a. Wood decay and nutrient partitioning by the cord forming basidiomycete *Phanerochaete velutina*: the significance of local nutrient supply. *New Phytologist* **138**: 607–617.

Wells JM, Boddy L, Evans R. 1995. Carbon translocation in mycelial cord systems of *Phanerochaete velutina* (DC. Pers.) Parmasto. *New Phytologist* **129**: 467–476.

Wells JM, Harris MJ, Boddy L. 1998b. Temporary phosphorus partitioning in mycelial systems of the cord-forming basidiomycete *Phanerochaete velutina*. *New Phytologist* **140**: 283–293.

Wells JM, Harris MJ, Boddy L. 1999. Dynamics of mycelial growth and phosphorus partitioning in developing *Phanerochaete velutina*: dependence on carbon availability. *New Phytologist* **142**: 325–334.

Wells JM, Hughes C, Boddy L. 1990. The fate of soil-derived phosphorus in mycelial cord systems of *Phanerochaete velutina* and *Phallus impudicus*. *New Phytologist* **114**: 595–606.